



POTSDAM-INSTITUT FÜR
KLIMAFOLGENFORSCHUNG

Originally published as:

Zheng, X., Li, Y., [Kurths, J.](#), Xu, Y. (2024): Noise-induced stochastic switching of microcargoes transport in artificial microtubule. - Chaos, 34, 9, 091101.

DOI: <https://doi.org/10.1063/5.0226188>

RESEARCH ARTICLE | SEPTEMBER 05 2024

Noise-induced stochastic switching of microcargoes transport in artificial microtubule

Xinwei Zheng ; Yongge Li ; Jürgen Kurths ; Yong Xu  



Chaos 34, 091101 (2024)

<https://doi.org/10.1063/5.0226188>



Articles You May Be Interested In

Experiments with microrods in a radio-frequency plasma sheath

Phys. Plasmas (June 2006)

In-situ scanning electron microscopy and atomic force microscopy Young's modulus determination of indium oxide microrods for micromechanical resonator applications

Appl. Phys. Lett. (April 2014)

Nonlinear dynamics of C-terminal tails in cellular microtubules

Chaos (July 2016)



Chaos

Special Topics Open
for Submissions

[Learn More](#)



Noise-induced stochastic switching of microcargoes transport in artificial microtubule

Cite as: Chaos 34, 091101 (2024); doi: 10.1063/5.0226188

Submitted: 30 June 2024 · Accepted: 20 August 2024 ·

Published Online: 5 September 2024



View Online



Export Citation



CrossMark

Xinwei Zheng,¹ Yongge Li,^{1,2} Jürgen Kurths,^{3,4} and Yong Xu^{1,5,a)}

AFFILIATIONS

¹School of Mathematics and Statistics, Northwestern Polytechnical University, Xi'an 710072, China

²Research and Development Institute of Northwestern Polytechnical University in Shenzhen, Shenzhen City, 518063, China

³Potsdam Institute for Climate Impact Research, Potsdam 14412, Germany

⁴Department of Physics, Humboldt University Berlin, Berlin 12489, Germany

⁵MOE Key Laboratory for Complexity Science in Aerospace, Northwestern Polytechnical University, Xi'an 710072, China

^{a)}Author to whom correspondence should be addressed: hsux3@nwpu.edu.cn

ABSTRACT

Synchronization plays an important role in propelling microrobots, especially for those driven by an external magnetic field. Here, we substantially contribute to the understanding of a novel out-of-sync phenomenon called “slip-out”, which has been recently discovered in experiments of an artificial microtubule (AMT). In a deterministic situation, we interpret and quantitatively characterize the switching in such a system between the stick and slip modes, whose different combinations over time define four long-term states. The stick-and-slip state is the most typical “slip-out” state with periodic switching, caused by both the phase lock between the microrod and the magnetic field, and the time-dependent magnetic moment. We then illustrate that thermal noise leads to stochastic switching by stimulating the phase difference across a specific threshold randomly. Finally, we reproduce the average velocity simulatively, which is highly consistent with real experiments. Importantly, the nearly permanent slip state is probed by our analysis of long-term states rather than observing real experiments. The investigation supports the design and operational strategies of AMT and other microrobots driven by magnetic fields.

Published under an exclusive license by AIP Publishing. <https://doi.org/10.1063/5.0226188>

Microrobots are devices designed to achieve functions in mobile robotic systems of a sub-millimeter range, for example, moving in complex media, responding to the environment and self-organizing.^{1,2} An external rotating magnetic field is often applied to actuate magnetic microrobots by making them rotating simultaneously with the external field. However, a phenomenon called “step-out” breaks the synchronization between the microrobots and the external field. This phenomenon was initially and commonly discovered in experiments of spiral propellers,^{3,4} characterized by the synchronous rotation (with a constant phase lag) or an out of sync rotation (with a time-dependent phase lag) with the external field when the field's frequency is below or above the critical “step-out” frequency, respectively. The Artificial microtubule (AMT) is a recently designed strategy for rapid and robust transport of microcargoes, whose experiments perform both the “step-out” phenomenon and a novel translationally out-of-sync phenomenon called “slip-out.” Here, we will describe the “slip-out” phenomenon in detail and propose the complete

mechanisms of it, aiming to improve the system's performance and enrich the understanding of slippage phenomena.

I. INTRODUCTION

Transport of particles within living organisms is significant and stimulates progressive development of microrobotic delivery technologies.^{5,6} In particular, AMT has been recently designed to achieve the robust and collective transport of micromagnetic colloids.⁷ This technology is inspired by cytoskeletal motors that carry vesicles along microtubule highways in cells.⁸ During the one-step transport of the slender microrod with a length l , one of its end is fixed on equidistant stepping stones on the AMT, and the entire body rotates on the AMT controlled by an external rotating magnetic field. Such a transient translation mode is called the stick mode. This process repeats until the microrod is horizontally placed and the other end is also fixed on the next stepping stone [Fig. 1(a)].

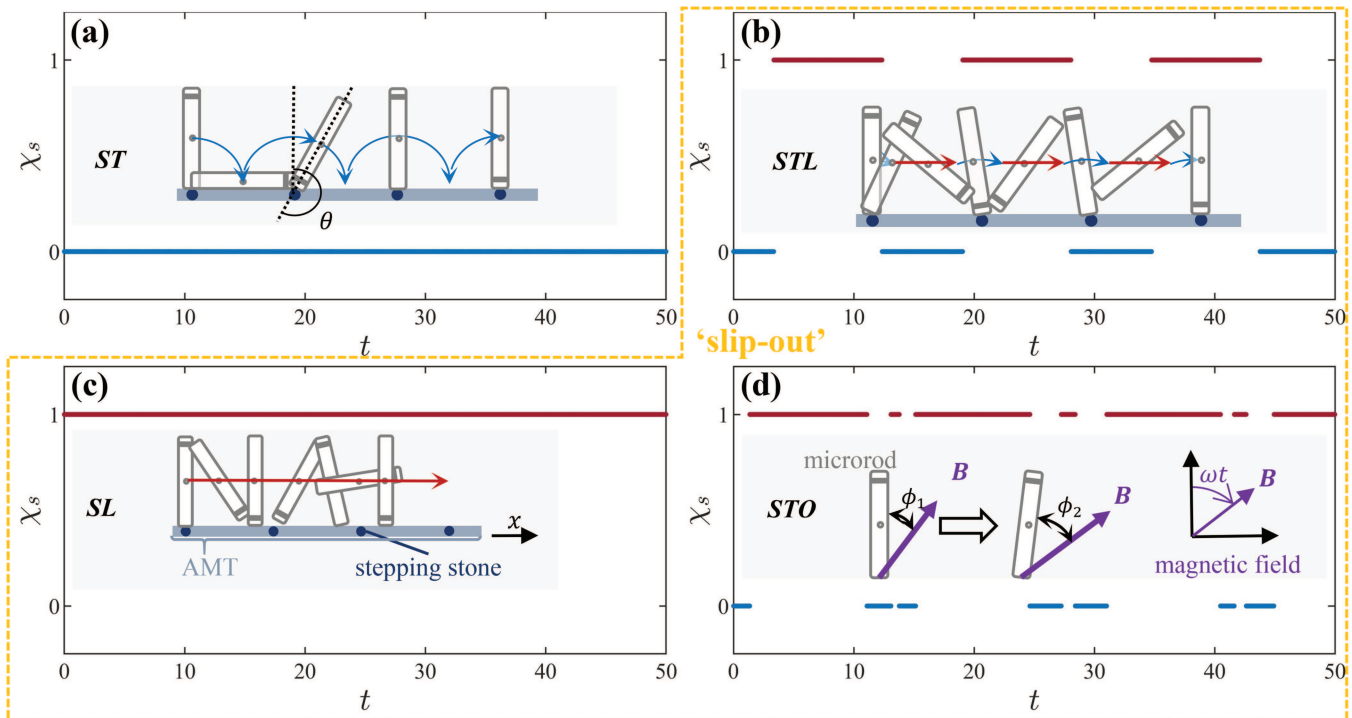


FIG. 1. Schematic diagrams of four long-term states and variation of $\chi_s(t)$ with different (ϕ_m, ω) . The gray rectangles are conceptual microrods moving on AMT. In the first three states, the microrod rotates clockwise with the external rotating magnetic field. (a) In the ST state ($\phi_m = 0.5, \omega = 0.2$), the microrod attaches to the stepping stones constantly and moves toward right. The motions are the same to the ST state when the microrod attaches to the stepping stones. (b) In the STL state ($\phi_m = 0.2, \omega = 0.4$), the microrod periodically disengages from the stepping stones and proceeds slower toward right. (c) In the SL state ($\phi_m = 0.15, \omega = 0.7$), the microrod never attaches to the stepping stones as it rotates and proceeds rightward. (d) In the STO state ($\phi_m = 0.5, \omega = 1.0$), the microrod sometimes rotates counterclockwise and attaches to the stepping stones intermittently.

As the rotation continues, the originally fixed end starts to rise from the AMT. Sequentially, the continuous rotation converts to the step-by-step motion and causes a displacement of the microrod. This expected long-term state is called the stick state (ST). Compared to existing magnetic microbotic transport methods with various locomotion mechanisms, the AMT generates a higher dimensionless velocity.^{9–12}

As has been discovered very recently,⁷ microrods transported by the AMT suffer from the translationally asynchronization phenomenon when the rotating frequency of the magnetic field is relatively high. This interesting phenomenon is called “slip-out”, consisting of three typical long-term states, i.e., the stick-and-slip state (STL) with periodic departure from stepping stones, the permanent slip state (SL) with permanent departure, and the step-out state (STO) in which the microrod falls out of step with the magnetic field [Figs. 1(b)–1(d)]. Obviously, “slip-out” damages the robustness of AMT, especially for the collective transport. As a result, it is essential to reveal the underlying mechanism and achieve a better transport performance. The original research revealed that the critical “slip-out” frequency is proportional to the square of the external magnetic field intensity (see the supplementary material in Ref. 7). However, neither the switching in the stick-and-slip state nor the variation of

the average velocity could be explained in Ref. 7. Consequently, the understanding of the phenomena mentioned above is a challenging and open problem, which we will treat in this contribution.

Stochastic disturbance widely exists in various systems and has a remarkably impact on their dynamics, from macroscopic airfoil^{13,14} to micro-electromechanical systems¹⁵ and microscopic particles.^{16,17} As for the transport of microrobots, due to their ultratiny size, they are inevitably influenced by thermal noise, resulting in the randomness of both their translation and orientation.^{18–22} Particularly, the experimental results of the AMT are surprisingly different between groups even under the same conditions [Figs. 3(a) and 3(b) in Ref. 7], which is impossible under deterministic circumstances. Specifically, in a single experiment, the microrod exhibits both unexpected flip-back behavior in orientation and rare departure from stepping stones with a relatively low frequency of the rotating magnetic field [see supplementary video 3 (5 mT, 0.3 Hz) in Ref. 7]. Consequently, it is reasonable to attribute the phenomena to the influence of thermal noise.

Here, we contribute to the deep understanding of the switching in the AMT both in deterministic and stochastic cases. The four long-term states are analyzed by different switching mechanisms between the stick and the slip modes. Our model successfully

reproduces the results from real experiments, as we will illustrate later in detail.

II. MECHANISMS OF THE “SLIP-OUT” PHENOMENON

In fact, the complex movements of a microrod can be decomposed into two simple behaviors, i.e., the rotation behavior and the adsorption behavior to the stepping stone. It will subsequently be uncovered that how the microrod adsorbs on the AMT when it rotates. For the rotation behavior, the microrod is forced to rotate by the magnetic moment $MB \sin(\omega t - \theta)$ generated by the external magnetic field ($T_M = |MB \sin(\omega t - \theta)|$), in which M, θ represent the magnetization and the orientation of the microrod, and B, ω represent the intensity and angular velocity of the external rotating magnetic field.

A. Out-of-sync behavior in rotation

In the absence of noise, the rotational dynamics is governed by $J\dot{\theta} + \gamma\dot{\theta} = MB \sin(\omega t - \theta)$, in which J, γ are the moment of the inertia and the drag coefficient. In the overdamped environment, the inertial term is far less than the damping term and can be neglected. By introducing the constant $\omega_c = MB/\gamma$, the above governing equation can be converted to $\dot{\theta} = \omega_c \sin(\omega t - \theta)$, equivalent to an Adler-like equation,^{23,24}

$$\dot{\phi} = \omega - \omega_c \sin \phi, \tag{1}$$

in which $\phi = \omega t - \theta$. When $\omega \leq \omega_c$, system (1) has a stable node $\phi_s = \arcsin \omega/\omega_c$ and an unstable saddle $\phi_u = \pi - \arcsin \omega/\omega_c$. In this case, $\sin(\phi)$ converges to ω/ω_c with all initial conditions, namely, $\theta = \omega t - \phi_s$. This indicates that when ω is not large enough, the microrod spins synchronously with the rotation of the external magnetic field, as shown in Fig. 2(a) ($\omega = 0.1, 0.4, 0.7, 1.0$). When $\omega > \omega_c$, system (1) has no stable point and $\sin(\phi)$ will keep changing, which results in a time-changing angular difference between the rotation of the microrod and the external magnetic field, as shown in Fig. 2(a) ($\omega = 1.3, 1.6$). In this case, the microrod rotates slower with growing ω , and the angular velocity difference between the microrod and the external field increases [Fig. 2(b)]. Opposite to the previous situation, in this case, they rotate out of sync.^{4,25} This parameter-dependent phenomenon is related to the bifurcation theory in nonlinear dynamics, which is applied to a variety of systems in real world.^{26–28} We describe the saddle-node bifurcation of system (1) in Fig. 2(c).

B. Relation between the rotation and the absorption

For the absorption regime, a non-negligible magnetic moment (denote its absolute value as T_S) to the microrod is generated when its ends close to the stepping stone. Obviously, its one end will absorb onto the stepping stones if $T_S \geq T_M$. For example, in the *ST* state, the microrod touches the stepping stone periodically with θ , indicating that T_S also changes periodically with the rotation of an external magnetic field. Thus, for simplicity, we assume $T_S = MB(c_1 + c \cos \omega t)$, $c + 1 > c_1 > c > 0$. Note that in Ref. 7, the magnetic field generated by the stepping stone is also periodic, supporting the above assumption. To compare easily with T_M , we substitute $\arcsin(c_1 - c)$ with ϕ_m and obtain $T_S = MB[\sin \phi_m$

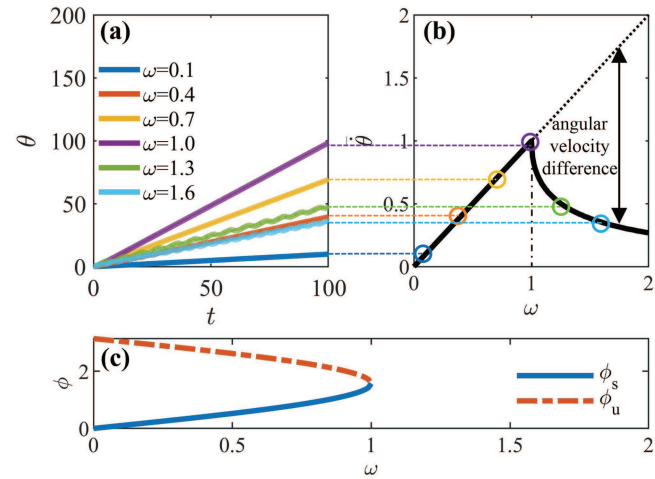


FIG. 2. Quantitative descriptions of the “step-out” phenomenon. (a) Plots of θ against t with different ω . (b) Plots of an average angular velocity of the microrod (solid line) and the external field (dashed line) against ω . (c) The bifurcation diagram of system (1). $\omega_c = 1$.

$+ c(\cos \omega t + 1)]$. Then, the main task becomes the comparison between T_S and T_M . The translation mode is determined by the comparison between T_S and T_M and represented by a 0-1 time-dependent variable $\chi_s(t)$,

$$\chi_s(t) = \begin{cases} 0, & T_M \leq T_S, \text{ stick mode,} \\ 1, & T_M > T_S, \text{ slip mode.} \end{cases} \tag{2}$$

By eliminating MB , $T_M > T_S$ reduces to

$$|\sin \phi| > \sin \phi_m + c(\cos \omega t + 1). \tag{3}$$

This inequality holds in various regimes with changing ω , corresponding to different translation states of the microrod.

C. Division of long-term states

In the following, we divide the domain of ω into four parts. (i) For $\omega \in [0, \omega_c \sin \phi_m]$, Eq. (3) never holds; thus, the microrod rotates forward permanently in the stick mode. In this state, $\chi_s(t) \equiv 0$ [Fig. 1(a)]. (ii) For $\omega \in (\omega_c \sin \phi_m, \omega_c(\sin \phi_m + 2c)]$, Eq. (3) periodically holds, indicating that the microrod rotates forward periodically in the stick and the slip modes. In this state, $\chi_s(t)$ periodically switches between 0 and 1 [Fig. 1(b)]. (iii) For $\omega \in (\omega_c(\sin \phi_m + 2c), \omega_c]$, Eq. (3) holds for any t , indicating that the microrod rotates forward only in the slip mode. In this state, $\chi_s(t) \equiv 1$ [Fig. 1(c)]. (iv) For $\omega \in (\omega_c, +\infty)$, Eq. (3) holds intermittently but not periodically. In this state, $\chi_s(t)$ irregularly switches between 0 and 1 [Fig. 1(d)].

In order to quantify the above analysis, we propose P_{sl} as the strength of the “slip-out”,

$$P_{sl} = \lim_{t \rightarrow \infty} \frac{1}{t} \int_0^t \chi_s(t) dt. \tag{4}$$

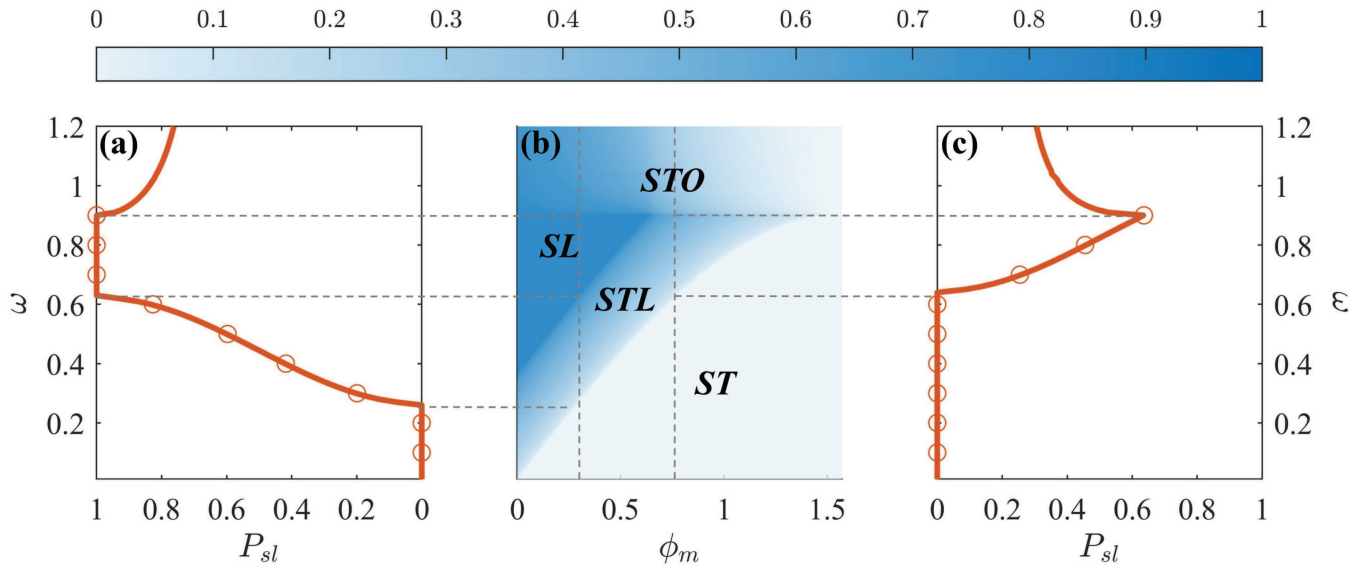


FIG. 3. The variation of the “slip-out” strength P_{sl} with ω and ϕ_m and the division of long-term states based on the value of P_{sl} . (a) The variation of P_{sl} as a function of ω (experiences all four long-term states); solid line: numerical results and circles: analytical results by Eq. (11), $\phi_m = 0.3$. (b) Value of P_{sl} on the (ϕ_m, ω) plane and regions of the long-term states. (c) The variation of P_{sl} as a function of ω (experiences three long-term states: ST , STL , and STO); solid line: numerical results, circles: analytical results by Eq. (11), $\phi_m = 0.8$, $\omega_c = 0.9$.

Obviously, $P_{sl} = 1$ for the SL state and $P_{sl} = 0$ for the ST state. In the STL state,

$$P_{sl} = \pi^{-1} \arccos[c^{-1}(\omega/\omega_c - \sin \phi_m) - 1], \quad (5)$$

which is obtained by calculating the proportion that Eq. (3) holds with increasing ωt from 0 to 2π .

In Fig. 3(b), from the heat map with respect to (ϕ_m, ω) , when $\sin \phi_m + 2c < 1$, the microrod goes through all the four states: P_{sl} keeps at 0 in the ST state, increases monotonically in the STL state until reaching 1 in the SL state, while decreases in the STO state [Fig. 3(a)]. However, when $\sin \phi_m + 2c \geq 1$, with increasing ω , the SL state disappears. The microrod only experiences three states, i.e., a large region of the ST state, a narrow region of the STL state, and then the STO state [Fig. 3(c)]. It should be emphasized that although the SL state may exist theoretically, it can be hardly detected in real experiments, which we will illustrate later. Except this, we can still claim that our results are consistent with real experiments.

D. Translation characteristics of long-term states

With different states, the translation velocity also differs. In the ST state, the microrod rotates forward step-by-step, whose translation velocity can be easily derived as

$$\dot{x}_{st} = \frac{1}{2} l \omega_c \sin(\omega t - \theta) |\cos \theta|. \quad (6)$$

While in the SL state, the microrod never touches the stepping stone, and its translational movement, in fact, originates from the near-wall effect.^{7,29} Consider that the microrod rotates regularly, the

translational velocity can be simplified as

$$\dot{x}_{sl} = \lambda \omega_c \sin(\omega t - \theta), \quad (7)$$

in which λ is a constant. In Fig. 4, the responses for these states are illustrated. For the STL and the STO states, the displacement is

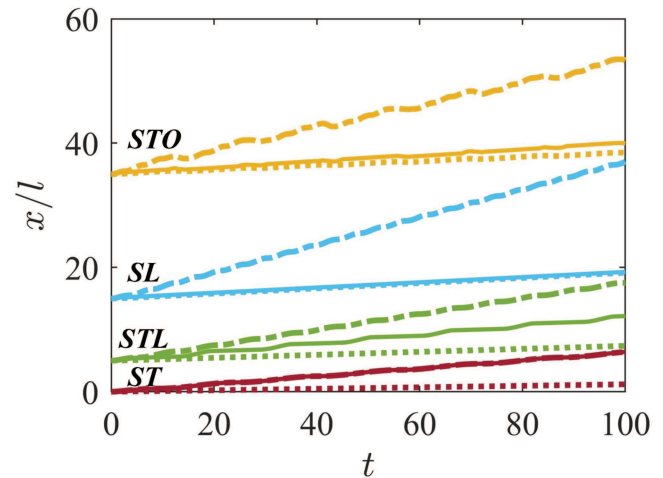


FIG. 4. Plots of the normalized displacement of the microrod x/l as t grows in four states, solid lines: real displacements, dashed lines: ideal displacements in the SL state, dashed-dotted lines: ideal displacements in the ST state, $\lambda = 0.06$, $c = 0.2$. For convenience, the transient dynamics is neglected by setting the initial condition at the stable point $\phi_s = \arcsin \omega/\omega_c$ throughout the article if $\omega \leq \omega_c$.

combined with alternating x_{st} and x_{sl} . Particularly, *STO* corresponds to the back-and-forth displacement according to the “step-out” phenomenon.

III. EFFECT OF THERMAL NOISE

A. Stochastic switching

The above analyses are based on the deterministic assumption. However, the microrod is inevitably disturbed by thermal noise due to its micro size, which may act either on the rotational dynamics or the translational movement. With the stochastic excitation on θ , the microrod no longer rotates regularly. Consequently, it is difficult to clarify the absolute stick or slip states. In addition, in case (ii), the two modes switch randomly rather than periodically in the deterministic case. To describe this phenomenon, the governing equation for the orientation is rewritten as $J\ddot{\theta} + \gamma\dot{\theta} = MB \sin(\omega t - \theta) + \xi$, in which ξ is Gaussian white noise. Considering an overdamped environment, the equation reduces to

$$\dot{\phi} = \omega - \omega_c \sin \phi + \xi, \tag{8}$$

in which ξ is Gaussian white noise with $\langle \xi(t) \rangle = 0$ and $\langle \xi(t)\xi(t + \tau) \rangle = 2D\delta(\tau)$ and D is the noise intensity.

Equation (8) can be viewed as a tilted ratchet dynamical system,³⁰ where the potential energy is $U(\phi) = -(\omega\phi + \omega_c \cos \phi)$. Under the excitation of noise, the system will fluctuate at the bottom of each potential well or even cross the unstable point rather than keeping still,³¹ as shown by the hollow particles in Fig. 5(a). Correspondingly, the stochastic switch between the stick and the slip modes may happen even when $\omega < \omega_c \sin \phi_m$, which is impossible for the deterministic case, as illustrated by the solid particle in Fig. 5(a). This is, in fact, the noise-induced transition over a time-varying threshold related to $\sin \phi_m + c(\cos \omega t + 1)$, which indicates that the switching requires at least $\phi > \phi_m$ or $\phi < -\phi_m$. Specifically, in Fig. 5(b), as D changes from 0 to 10^{-2} , the switching frequency increases greatly. However, it is impossible to visually determine the proportion of the two modes when D is large.

To determine the proportion of the slip mode in the stochastic case, the most important problem is calculating the probability density function³² (PDF) of ϕ . Commonly, the PDF can be achieved by solving the Fokker–Planck (FP) equation.³³ The corresponding probability density p for system (8) obeys the FP equation $\partial p / \partial \tau = -\partial J / \partial \phi$, in which the probability current $J = (\omega / \omega_c + \sin \phi)p - \partial(Dp) / \partial \phi$.

We restrict $\phi \in (-\pi, \pi)$ and use a periodic boundary condition $p(-\pi) = p(\pi)$. Then, the solution of the FP equation for system (8) is³⁴

$$p(\phi) = C \frac{\psi(\phi)}{2D} \left\{ 1 - \left[1 - \frac{\psi(-\pi)}{\psi(\pi)} \right] \frac{\int_{-\pi}^{\pi} \psi^{-1}(u) du}{\int_{-\pi}^{\pi} \psi^{-1}(u) du} \right\}, \tag{9}$$

in which $\psi(\phi) = \exp \left[\int_{\phi_0}^{\phi} 1/D(\omega/\omega_c - \sin \phi) d\phi \right]$. The explicit expression of $\psi^{-1}(u)$ is difficult to obtain. Thus, $p(\phi)$ is given either by numerical methods³³ or estimated by

$$p_1(\phi) \approx C\psi(\phi)/2D, \tag{10}$$

with small enough ω and D , in which C is a normalization constant. Considering the effect of noise, we propose $P_{sl}^* = \lim_{t \rightarrow \infty} \frac{1}{t} \int_0^t \chi_s(t) dt$. Generally, P_{sl} as a function of ω is obtained by $P_{sl}(\omega) = \int_{-\pi}^{\pi} p(\phi) \cdot P_{sl}(\phi) d\phi$, in which $P_{sl}(\phi)$ can be calculated directly from Eq. (3). The analytical expressions of P_{sl} are worked out with $p(\phi) = \delta(\phi - \phi_c)$ when $\omega \leq \omega_c$. We generalize this form to estimate P_{sl}^* theoretically, with $\phi \in [-\pi/2, \pi/2]$ due to the limitation of ω . Both ϕ and $-\phi$ correspond to the same P_{sl} according to Eq. (3). Therefore, P_{sl}^* can be estimated by

$$P_{sl}^* \approx \int_{-\pi/2}^{-\phi_m} p_1(\phi) \cdot P_{sl}(-\phi) d\phi + \int_{\phi_m}^{\pi/2} p_1(\phi) \cdot P_{sl}(\phi) d\phi, \tag{11}$$

with small enough ω and D [Fig. 5(c)]. The probability of $|\phi| > \pi/2$ increases with growing ω and D , which is excluded by our estimation and causes a decline of the accuracy of Eq. (11).

For small ω , such as within case (i), the system originally stays in the stick mode. The smaller the ω , the more it requires for the system to reach the threshold from ϕ_c . This means that the probability of switching from the stick mode to the slip mode is very small. However, with increasing noise intensity D , the switching becomes easier. Oppositely, for large ω , such as within case (iii), the system originally stays in the slip mode. A larger ω indicates that it is more difficult for the system to switch from the slip mode to the stick mode. For a moderate ω , noise only makes the switching more frequent while not changes the proportion apparently [Fig. 5(d)].

B. Reproducing results of real experiments

In addition, thermal noise directly affects the displacement. We introduce the stochastic forces as Gaussian white noise ξ_1, ξ_2 in the dynamic models of translation,

$$\dot{x}_{st} = \frac{1}{2} l \omega_c \sin(\omega t - \theta) |\cos \theta| + \xi_1(t) \tag{12}$$

and

$$\dot{x}_{sl} = \lambda l \omega_c \sin(\omega t - \theta) + \xi_2(t). \tag{13}$$

In these equations, $\xi_i(t)$ are the Gaussian white noise, with $\langle \xi_i(t) \rangle = 0$, $\langle \xi_i(t)\xi_j(t + \tau) \rangle = 2D_{ij}\delta_{ij}\delta(\tau)$, $\langle \xi_i(t)\xi(t + \tau) \rangle = 0$, in which D_{ij} is the noise intensity ($i, j = 1, 2$). We use the frequencies f, f_c (in Hz) instead of the angular velocities ω, ω_c (in rad) to maintain consistency with the parameters in real experiments. The frequency (“step-out” frequency) is related to the angular velocity (“step-out” angular velocity) by $f = \omega / 2\pi$ ($f_c = \omega_c / 2\pi$). The noise strength is set as $D_{11} < D_{22} \ll D$. The relation $D_{11} < D_{22}$ originates from the strong anchoring effect of stepping stones in the stick mode, and $D_{22} \ll D$ is due to the magnitude difference between orientation and displacement. A previous study showed that $M \propto B$ for a slender ellipsoid.³⁵ Therefore, we approximate $f_c \propto B^2$ for the microrod. We set the critical frequencies $f_{ck} = 0.9 \times 4^{k-1}$ Hz ($k = 1, 2, 3$) to keep consistent with different B in real experiments. The average velocity and the dimensionless average velocity can be computed as $v = \bar{\dot{x}}$ and $Z = v/(fL)$, respectively.

The variation of v and Z is characterized by our simulations and interpreted by our theoretical analysis. We demonstrate the variation of v in Fig. 6(a) with different f_c , which is consistent with the results of real experiments [Fig. 3(a) in Ref. 7]. The curve $v = 2fl$

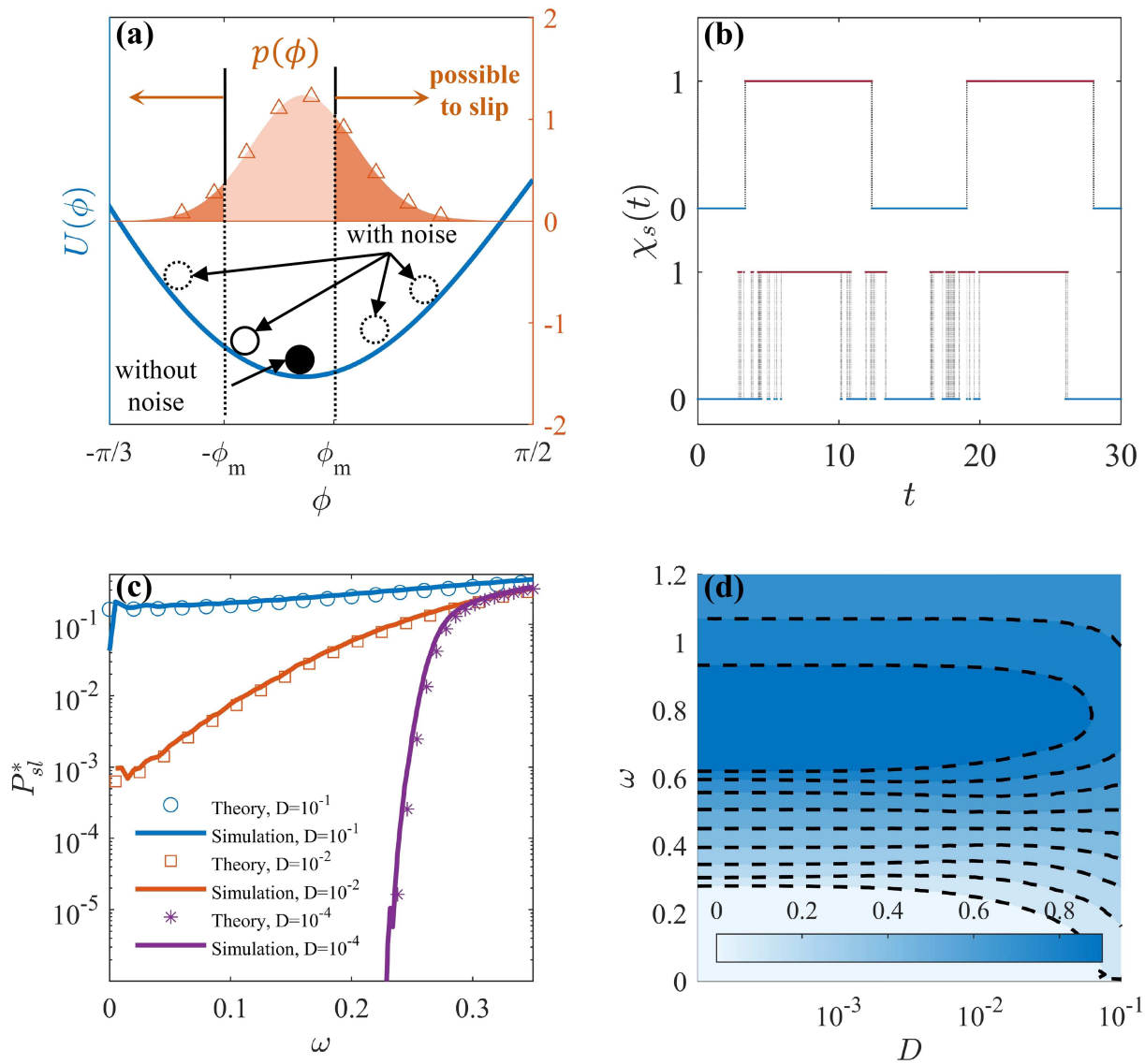


FIG. 5. The schematic diagram and results of the effect of thermal noise on the switching. (a) Diagram of the value of ϕ and its possibility to cross $\pm\phi_m$ with and without noise, blue line: the potential $U(\phi)$, orange area: the PDF of system (8), triangles: the estimated analytical solution (10), $\omega_c = 1.0, \omega = 0.15, \phi_m = \arcsin 1/3, D = 0.1$. (b) Plots of $\chi_s(t)$, $D = 0$ (upper), 10^{-2} (lower), respectively, $\omega_c = 0.9, \omega = 0.4, \phi_m = 0.2$. (c) Plots of P_{sl}^* numerically (solid lines) and by Eq. (11) (markers). (d) Contour map of P_{sl}^* on the (D, ω) plane, the contour interval is 0.1, $\omega_c = 0.9, \phi_m = \arcsin 0.3$.

corresponds to situations where the proportion of the slip mode is almost negligible (named as the ST^* state). Therefore, the average velocity can be estimated by

$$v_{st} = \lim_{t \rightarrow \infty} \frac{1}{t} \left(\int_0^t \frac{1}{2} l \omega_c \sin(\omega t - \theta) |\cos \theta| dt + \int_0^t dB_1 \right) = 2fl. \tag{14}$$

Similarly, the curve $v = 2\pi\lambda fl$ corresponds to situations where the proportion of the stick mode is negligible (named as the SL^* state).

Therefore, the average velocity can be estimated by

$$v_{sl} = \lim_{t \rightarrow \infty} \frac{1}{t} \left(\int_0^t \lambda l \omega_c \sin(\omega t - \theta) dt + \int_0^t dB_2 \right) = 2\pi\lambda fl. \tag{15}$$

The corresponding v between the above two curves represents the situations where the proportion of both modes is not negligible (named as the STL^* state), in which the fluctuations of v are attributed to the increasing f and P_{sl}^* . In this case, the average velocity

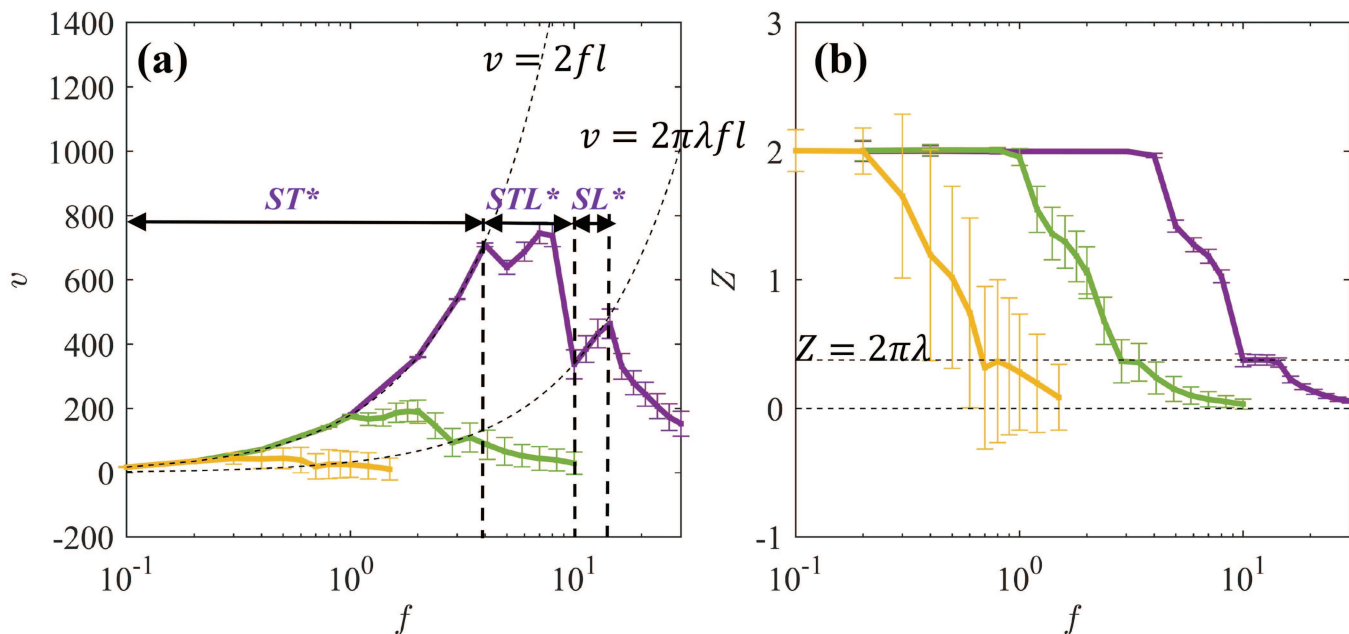


FIG. 6. Plots of (a) the average velocity v ($\mu\text{m/s}$) and (b) the dimensionless average velocity Z as the magnetic field frequency f grows. Yellow solid lines: $f_{c1} = 0.9$ Hz, green solid lines: $f_{c2} = 3.6$ Hz, and purple solid lines: $f_{c3} = 14.4$ Hz. $D_{11} = 10^{-11}$, $D_{22} = 10^{-8}$, $D = 10^{-2}$, $l = 9 \times 10^{-8}$ m, $\phi_m = \arcsin 0.3$, $c = 0.2$. The error bars are based on 20 repeated numerical simulations.

can be expressed by

$$v = 2fl \cdot (1 - P_{sl}^*) + 2\pi\lambda fl \cdot P_{sl}^* \tag{16}$$

With increasing P_{sl}^* and f , the average velocity will decrease and increase, respectively. However, the increase in f and P_{sl}^* happens simultaneously; therefore, the average velocity does not change monotonically. Note that in real experiments, the SL^* state is hard to be observed directly. However, interestingly, if $v = 2\pi\lambda fl$ is drawn on the velocity graph [Fig. 3(a) in Ref. 7] with a proper λ , such situations can be revealed.

The variation of Z can be interpreted in the same way as v . The curve $Z = 2$ corresponds to the ST^* state, in which $Z = 2$. The fluctuations around $Z = 2\pi\lambda$ correspond to the SL^* state. The surrounded part by the above lines corresponds to the STL^* state, in which Z experiences a slow decrease and then a rapid one as f grows [Fig. 6(b)].

IV. CONCLUSIONS

In conclusion, we have investigated the essence of the “slip-out” behavior and the effect of noise on the switching between two translation modes. We understand the switching mechanism by a competition of magnetic moments provided by the external rotating magnetic field and stepping stones, respectively. The proportion of the slip mode is represented by P_{sl} and based on its different translation properties as ω grows. We define four long-term translation states, in which the STL state is the most typical “slip-out” state with periodic switching. Furthermore, we include thermal noise to the

system and find that it increases the frequency of switching. The effect of noise is then quantitatively described by P_{sl} and the solution of PDF. Finally, we illustrate the variation of the average velocity and the dimensionless average velocity numerically, which is consistent with real experiments. We stress that we reveal evidence that the SL^* state exists by analyzing the curves $v = 2\pi\lambda fl$ in both our simulations and in real experiments.

Although found and named in the AMT experiments for the first time, the “slip-out” phenomenon can find its similarity in a wide range of systems, for example, slippage in tires,³⁶ gear rolling,³⁷ and bipedal robots.³⁸ We believe that this research substantially enriches the understanding of slippage phenomena in other systems in real world.³⁹

ACKNOWLEDGMENTS

This work was partly supported by the Key International (Regional) Joint Research Program of the NSF of China under Grant No. 12120101002 and the NSF of China under Grant No. 12072264. Y.L. thanks the NSF of China for support under Grant No. 12272296, the NSF of Chongqing, China under Grant No. cstc2021jcyj-msxmX0738, and the NSF of Guangdong Province, China under Grant No. 2023A1515012329.

AUTHOR DECLARATIONS

Conflict of Interest

The authors have no conflicts to disclose.

Author Contributions

Xinwei Zheng: Conceptualization (equal); Investigation (lead); Validation (equal); Visualization (lead); Writing – original draft (lead); Writing – review & editing (equal). **Yongge Li:** Conceptualization (lead); Methodology (equal); Supervision (equal); Validation (lead); Writing – original draft (equal); Writing – review & editing (equal). **Jürgen Kurths:** Conceptualization (equal); Supervision (equal); Writing – review & editing (equal). **Yong Xu:** Conceptualization (lead); Methodology (lead); Project administration (lead); Supervision (lead); Writing – review & editing (equal).

DATA AVAILABILITY

The data that support the findings of this study are available from the corresponding author upon reasonable request.

REFERENCES

- 1 S. Palagi and P. Fischer, “Bioinspired microrobots,” *Nat. Rev. Mater.* **3**, 113–124 (2018).
- 2 L. Zhang, J. J. Abbott, L. Dong, B. E. Kratochvil, D. Bell, and B. J. Nelson, “Artificial bacterial flagella: Fabrication and magnetic control,” *Appl. Phys. Lett.* **94**, 064107 (2009).
- 3 M. Sendoh, N. Ajiro, K. Ishiyama, M. Inoue, K. Arai, T. Hayase, and J. Akedo, “Effect of machine shape on swimming properties of the spiral-type magnetic micro-machine,” *IEEE Trans. Magn.* **35**, 3688–3690 (1999).
- 4 A. W. Mahoney, N. D. Nelson, K. E. Peyer, B. J. Nelson, and J. J. Abbott, “Behavior of rotating magnetic microrobots above the step-out frequency with application to control of multi-microrobot systems,” *Appl. Phys. Lett.* **104**, 144101 (2014).
- 5 M. S. Anwar, G. K. Sar, M. Perc, and D. Ghosh, “Collective dynamics of swarmalators with higher-order interactions,” *Commun. Phys.* **7**, 59 (2024).
- 6 M. Gosak, M. Milojević, M. Duh, K. Skok, and M. Perc, “Networks behind the morphology and structural design of living systems,” *Phys. Life Rev.* **41**, 1–21 (2022).
- 7 H. Gu, E. Hanedan, Q. Boehler, T.-Y. Huang, A. J. T. M. Mathijssen, and B. J. Nelson, “Artificial microtubules for rapid and collective transport of magnetic microcargoes,” *Nat. Mach. Intell.* **4**, 678–684 (2022).
- 8 K. J. Verhey and J. W. Hammond, “Traffic control: Regulation of kinesin motors,” *Nat. Rev. Mol. Cell Biol.* **10**, 765–777 (2009).
- 9 O. S. Pak, W. Gao, J. Wang, and E. Lauga, “High-speed propulsion of flexible nanowire motors: Theory and experiments,” *Soft Matter* **7**, 8169 (2011), arxiv:1109.1631 [cond-mat, physics:physics].
- 10 M. Medina-Sánchez, L. Schwarz, A. K. Meyer, F. Hebenstreit, and O. G. Schmidt, “Cellular cargo delivery: Toward assisted fertilization by sperm-carrying micromotors,” *Nano Lett.* **16**, 555–561 (2016).
- 11 A. M. Maier, C. Weig, P. Oswald, E. Frey, P. Fischer, and T. Liedl, “Magnetic propulsion of microswimmers with DNA-based flagellar bundles,” *Nano Lett.* **16**, 906–910 (2016).
- 12 C. Peters, O. Ergeneman, P. D. W. García, M. Müller, S. Pané, B. J. Nelson, and C. Hierold, “Superparamagnetic twist-type actuators with shape-independent magnetic properties and surface functionalization for advanced biomedical applications,” *Adv. Funct. Mater.* **24**, 5269–5276 (2014).
- 13 W. Guo, Y. Xu, Y. Li, Q. Liu, and X. Liu, “Dynamic responses of a conceptual two-dimensional airfoil in hypersonic flows with random perturbations,” *J. Fluids Struct.* **121**, 103920 (2023).
- 14 Q. Liu, Y. Xu, J. Kurths, and X. Liu, “Complex nonlinear dynamics and vibration suppression of conceptual airfoil models: A state-of-the-art overview,” *Chaos* **32**, 062101 (2022).
- 15 D. Zhao, Y. Li, Y. Xu, Q. Liu, and J. Kurths, “Extreme events in a class of nonlinear Duffing-type oscillators with a parametric periodic force,” *Eur. Phys. J. Lett.* **137**, 314 (2022).
- 16 Y. Li, R. Mei, Y. Xu, J. Kurths, J. Duan, and R. Metzler, “Particle dynamics and transport enhancement in a confined channel with position-dependent diffusivity,” *New J. Phys.* **22**, 053016 (2020).
- 17 Y. Li, Y. Xu, J. Kurths, and X. Yue, “Lévy-noise-induced transport in a rough triple-well potential,” *Phys. Rev. E* **94**, 042222 (2016).
- 18 M. R. Edwards, R. Wright Carlsen, and M. Sitti, “Near and far-wall effects on the three-dimensional motion of bacteria-driven microbeads,” *Appl. Phys. Lett.* **102**, 143701 (2013).
- 19 D. Kim, A. Liu, E. Diller, and M. Sitti, “Chemotactic steering of bacteria propelled microbeads,” *Biomed. Microdevices* **14**, 1009–1017 (2012).
- 20 N. Koumakis, A. Lepore, C. Maggi, and R. Di Leonardo, “Targeted delivery of colloids by swimming bacteria,” *Nat. Commun.* **4**, 2588 (2013).
- 21 F. Hajizadeh, L. Shao, D. Andrén, P. Johansson, H. Rubinsztein-Dunlop, and M. Käll, “Brownian fluctuations of an optically rotated nanorod,” *Optica* **4**, 746 (2017).
- 22 P. V. Ruijgrok, N. R. Verhart, P. Zijlstra, A. L. Tchebotareva, and M. Orrit, “Brownian fluctuations and heating of an optically aligned gold nanorod,” *Phys. Rev. Lett.* **107**, 037401 (2011).
- 23 R. Adler, “A study of locking phenomena in oscillators,” *Proc. IRE* **34**, 351–357 (1946).
- 24 A. Cēbers and M. Ozols, “Dynamics of an active magnetic particle in a rotating magnetic field,” *Phys. Rev. E* **73**, 021505 (2006).
- 25 W. A. Shelton, K. D. Bonin, and T. G. Walker, “Nonlinear motion of optically torqued nanorods,” *Phys. Rev. E* **71**, 036204 (2005).
- 26 M. Ahmadian and S. Yang, “Hopf bifurcation and hunting behavior in a rail wheelset with flange contact,” *Nonlinear Dyn.* **15**, 15–30 (1998).
- 27 M. Ahmadian and S. Yang, “Effect of system nonlinearities on locomotive bogie hunting stability,” *Veh. Syst. Dyn.* **29**, 365–384 (1998).
- 28 Q. Liu, Y. Xu, and J. Kurths, “Bistability and stochastic jumps in an airfoil system with viscoelastic material property and random fluctuations,” *Commun. Nonlinear Sci. Numer. Simul.* **84**, 105184 (2020).
- 29 A. Chamolly, E. Lauga, and S. Tottori, “Irreversible hydrodynamic trapping by surface rollers,” *Soft Matter* **16**, 2611–2620 (2020).
- 30 Y. Li, Y. Xu, J. Kurths, and X. Yue, “Transports in a rough ratchet induced by Lévy noises,” *Chaos* **27**, 103102 (2017).
- 31 Y. Roongthumskul, R. Shlomovitz, R. Bruinsma, and D. Bozovic, “Phase slips in oscillatory hair bundles,” *Phys. Rev. Lett.* **110**, 148103 (2013).
- 32 D. Zhao, Y. Li, Y. Xu, Q. Liu, and J. Kurths, “Probabilistic description of extreme oscillations and reliability analysis in rolling motion under stochastic excitation,” *Sci. China Technol. Sci.* **66**, 2586–2596 (2023).
- 33 Y. Xu, H. Zhang, Y. Li, K. Zhou, Q. Liu, and J. Kurths, “Solving Fokker-Planck equation using deep learning,” *Chaos* **30**, 013133 (2020).
- 34 J. Q. Sun, *Stochastic Dynamics and Control*, Monograph Series on Nonlinear Science and Complexity (Elsevier, 2006), Vol. 4, pp. i–410.
- 35 J. J. Abbott, O. Ergeneman, M. P. Kummer, A. M. Hirt, and B. J. Nelson, “Modeling magnetic torque and force for controlled manipulation of soft-magnetic bodies,” *IEEE Trans. Robot.* **23**, 1247–1252 (2007).
- 36 J. P. Gray, V. V. Vantsevich, and J. Paldan, “Agile tire slippage dynamics for radical enhancement of vehicle mobility,” *J. Terramech.* **65**, 14–37 (2016).
- 37 J. Li, G. Wang, and T. Wu, “Numerical simulation and experimental study of slippage in gear rolling,” *J. Mater. Process. Technol.* **234**, 280–289 (2016).
- 38 B. Gamus and Y. Or, “Dynamic bipedal walking under stick-slip transitions,” *SIAM J. Appl. Dyn. Syst.* **14**, 609–642 (2015).
- 39 N. J. Córdova, B. Ermentrout, and G. F. Oster, “Dynamics of single-motor molecules: The thermal ratchet model,” *Proc. Natl. Acad. Sci. U.S.A.* **89**, 339–343 (1992).